



The Hohmann–Parker effect measured by the Mars Science Laboratory on the transfer from Earth to Mars: Consequences and opportunities



A. Posner^{a,*}, D. Odstrčil^{b,c}, P. MacNeice^b, L. Rastaetter^b, C. Zeitlin^d, B. Heber^e, H. Elliott^f, R.A. Frahm^f, J.J.E. Hayes^a, T.T. von Rosenvinge^b, E.R. Christian^b, J.P. Andrews^d, R. Beaujean^e, S. Böttcher^e, D.E. Brinza^g, M.A. Bullock^d, S. Burmeister^e, F.A. Cucinotta^h, B. Ehresmann^d, M. Epperly^f, D. Grinspoonⁱ, J. Guo^e, D.M. Hassler^d, M.-H. Kim^j, J. Köhler^e, O. Kortmann^k, C. Martin Garcia^e, R. Müller-Mellin^e, K. Neal^d, S.C.R. Rafkin^d, G. Reitz^l, L. Seimetz^e, K.D. Smith^f, Y. Tyler^f, E. Weigle^m, R.F. Wimmer-Schweingruber^e

^a NASA Headquarters, Science Mission Directorate, 300 E Street SW, Washington DC 20548, USA

^b NASA Goddard Space Flight Center, Code 674, 8800 Greenbelt Road, Greenbelt, MD 20771, USA

^c George Mason University, School of Physics, Astronomy, and Computational Sciences, 364 Research Hall, Fairfax, VA 22030-4444, USA

^d Southwest Research Institute, Space Science and Engineering Division, 1050 Walnut Street, Suite 300, Boulder, CO 80302, USA

^e Christian Albrechts Universität Kiel, Institut für Experimentelle und Angewandte Physik, Leibnizstr. 11, 24118 Kiel, Germany

^f Southwest Research Institute, Space Science and Engineering Division, 6220 Culebra Road, San Antonio, TX 78228, USA

^g Jet Propulsion Laboratory, California Institute of Technology, 4800 Oak Grove Drive, Pasadena, CA 91011, USA

^h University of Nevada, Las Vegas, Health Physics Department, Las Vegas, NV 89154, USA

ⁱ Denver Museum of Nature and Science, 2001 Colorado Boulevard, Denver, CO 80205, USA

^j NASA Johnson Space Center, 1601 NASA Parkway, Houston, TX 77058, USA

^k University of California, Berkeley, Space Science Laboratory, 7 Gauss Way, Berkeley, CA 94720, USA

^l Deutsches Zentrum für Luft- und Raumfahrt, Lindner Höhe, 51147 Köln, Germany

^m Big Head Endian LLC, 11785 181st Road, Burden, KS 67019, USA

ARTICLE INFO

Article history:

Received 23 May 2013

Received in revised form

16 August 2013

Accepted 16 September 2013

Available online 27 September 2013

Keywords:

Hohmann transit

Parker field

Magnetic connection

Cosmic rays

Solar wind

Inner heliosphere

ABSTRACT

We show that a spacecraft launched from Earth towards Mars following a Hohmann minimum energy transfer trajectory has a strong tendency to remain well-connected magnetically to Earth, in the early phase of the transfer, or to Mars in the late phase, via the Parker spiral magnetic field. On the return trip, the spacecraft would remain reasonably well-connected magnetically first to Mars and later to Earth. Moreover, good magnetic connectivity occurs on all Hohmann transfers between neighboring planets in the inner solar system out to Mars. We call this hitherto unnamed circumstance the Hohmann–Parker effect. We show consequences of the effect by means of simultaneous cosmic radiation proxy observations made near Earth, near Mars, and at the Mars Science Laboratory on the transfer from Earth to Mars in 2011/2012. We support the observations with simulations of the large-scale magnetic field of the inner heliosphere during this period and compare the results with our predictions. The implications of the Hohmann–Parker effect are discussed.

© 2013 Published by Elsevier Ltd.

* Corresponding author. Tel.: +1 202 358 0727.

E-mail addresses: arik.posner@nasa.gov (A. Posner), dusan.odstrcil@nasa.gov, dodstrcl@gmu.edu (D. Odstrčil), peter.j.macneice@nasa.gov (P. MacNeice), lutz.rastaetter@nasa.gov (L. Rastaetter), zeitlin@boulder.swri.edu (C. Zeitlin), heber@physik.uni-kiel.de (B. Heber), helliott@swri.edu (H. Elliott), rfrahm@swri.edu (R.A. Frahm), jhayes@nasa.gov (J.J.E. Hayes), tycho.t.vonrosenvinge@nasa.gov (T.T. von Rosenvinge), eric.r.christian@nasa.gov (E.R. Christian), andrews@boulder.swri.edu (J.P. Andrews), rudolf@rbeau.de (R. Beaujean), boettcher@physik.uni-kiel.de (S. Böttcher), david.e.brinza@jpl.nasa.gov (D.E. Brinza), bullock@boulder.swri.edu (M.A. Bullock), burmeister@physik.uni-kiel.de (S. Burmeister), francis.cucinotta@unlv.edu (F.A. Cucinotta), ehresmann@boulder.swri.edu (B. Ehresmann), mepperly@swri.edu (M. Epperly), dgrinspoon@dmns.org (D. Grinspoon), guo@physik.uni-kiel.de (J. Guo), hassler@boulder.swri.edu (D.M. Hassler), myung-hee.y.kim@nasa.gov (M.-H. Kim), koehler@physik.uni-kiel.de (J. Köhler), onno@ssl.berkeley.edu (O. Kortmann), martin@physik.uni-kiel.de (C. Martin Garcia), mueller-mellin@physik.uni-kiel.de (R. Müller-Mellin), kneal@boulder.swri.edu (K. Neal), rafkin@boulder.swri.edu (S.C.R. Rafkin), guenther.reitz@dlr.de (G. Reitz), seimetz@physik.uni-kiel.de (L. Seimetz), kdsmith@swri.edu (K.D. Smith), tyler@swri.edu (Y. Tyler), eddie@bigheadendian.com (E. Weigle), wimmer@physik.uni-kiel.de (R.F. Wimmer-Schweingruber).

1. Introduction

1.1. Defining the Hohmann–Parker effect

What we introduce as the Hohmann–Parker (HP) effect in this manuscript consists of the following set of predictions based on simple orbital analyses and idealized solar wind conditions. (1) We find that a transfer vehicle (TV) at any point on inbound and outbound Hohmann transfer orbits between neighboring planets in the inner solar system has small angular magnetic connection distances to one or the other planet. The magnetic connection distance is defined as the angular distance in longitude of the magnetic field line foot points on the solar source surface that connect two points in the heliosphere with the Sun. (2) The resulting latitudinal magnetic connection distances are small due to the small orbital inclinations of Laplace's invariable plane with respect to the solar rotation axis. The orbits of all inner solar system planets out to Mars also have small inclinations with respect to the Laplace invariable plane. Earth's inclination with respect to the solar equator is largest, at $\sim 7.2^\circ$. This number also is a good approximation for the largest latitudinal angular distance. 7.2° Separation can only be exceeded if the TV and the better-connected planet are beyond quadrature with the Sun, which does not occur during the transit. We therefore focus in the following on longitudinal magnetic separation distances. Here we distinguish between inner and outer magnetic connection distance (ICD and OCD), which refer to the nominal longitudinal separation of the magnetic foot points of the inner and the outer planet from the transfer vehicle, respectively, on the solar source surface.

On an outbound transfer (e.g., from Earth to Mars), the ICD is small at first. The ICD gradually increases over time, but before it can get large the TV reaches very small longitudinal magnetic connection distances with the arrival planet, i.e. a small OCD. Using idealized orbits and assuming typical solar wind conditions in which stream–stream interactions are neglected, the combination of magnetic field connections keeps the TV within 13° of angular distance from either of the two host planets.

On an inbound Hohmann transfer orbit (e.g., from Mars to Earth), the OCD remains small for most of the transfer. Near the end of the transfer, a small ICD will be established. The worst magnetic connection on the inbound trajectory would not exceed 25° assuming the simplified conditions.

The actual magnetic connection distance is a function of various factors that will be discussed, including solar wind speed variability, stream–stream interactions, orbital eccentricity and inclination, and value of semi-major axes of the planets involved. Also, recent developments in the improved understanding of the interplanetary magnetic field can have bearing on the magnetic connection distance.

The HP effect of small magnetic connection distances has very real consequences. A small magnetic connection distance means that between the two locations, the sources of the solar wind in a quasi-steady heliosphere are nearly co-located on the source surface of the Sun, which in most cases also means they are nearly co-located in the solar photosphere. This causes similar, correlated solar wind plasma, magnetic field and composition observations at both the TV and the planet with which its connection distance is smallest. Furthermore, magnetic fields guide and modulate energetic particles. Therefore, many aspects of galactic cosmic rays (GCRs) and energetic particles of solar origin will be closely related.

In November 2011, the Mars Science Laboratory was launched on a transfer from Earth to Mars, and it had a radiation detector on board that actively measured cosmic rays during the transfer. With proxy GCR observations also available near Earth and Mars, we will demonstrate the GCR aspect of the HP effect.

1.2. Pioneering achievements of Hohmann and Parker

Hohmann (1925) found the solution for interplanetary space travel after Goddard (1919) established that critical escape velocities could be attained with rocket combustion. One aspect of Hohmann's calculations concerns the minimum-energy solution for transferring a vehicle from planet to planet. This would be through accelerating a transfer vehicle onto an elliptical orbit with its perihelion at the inner planet and the aphelion at the outer planet's orbit. The aphelion would require additional acceleration of the transfer vehicle in order to land or reach an orbit about the arrival planet. The solutions put forward by Hohmann are the basis for all lunar and planetary exploration missions to this day. The first interplanetary application was Mariner 2 in 1962, which passed by Venus on December 14, 1962. Mariner 2 reached perihelion on December 27, slightly inside Venus' orbital radius, but no attempt to enter Venus orbit was planned for this mission. Among the many applications of this methodology toward planetary transfers, the successes of the missions Magellan to Venus and Viking (1 and 2), Pathfinder, Exploration Rover (Spirit and Opportunity) and now Mars Science Laboratory MSL (Curiosity) to Mars certainly stand out. It is possible that the methodology will be changed, as other missions now demonstrate small acceleration, e.g. by means of ion engines that provide constant, long-term acceleration. This aspect, however, is beyond the scope of our current work.

Parker (1958) predicted the existence of plasma streaming into interplanetary space as the extension of the hot solar corona. The extended solar atmosphere, now referred to as the solar wind, embeds all major planets and reaches out to at least 120 AU from the Sun (Decker et al., 2012), beyond which it encounters the interstellar medium, the plasma and neutral gas from other stars. The Sun has a latitude-dependent sidereal rotation period between 25.4 days near the equator and 30+ days at the poles. Magnetic fields are assumed to be the cause of the coronal temperature (2×10^6) exceeding by far the temperature of the photosphere ($\sim 5 \times 10^3$) below. Parker found that the enormous temperature of the corona would create plasma that exceeds the escape velocity of the solar gravitational field, and therefore is the underlying reason for the existence of the solar wind. Solar wind seemingly emanates from all heliolatitudes and longitudes, although active regions on the Sun maintain closed magnetic structures that would trap coronal plasma. Only above a certain height, $\sim 1.5R_s$, the so-called source surface, outflowing solar wind can be assumed to be present at all longitudes and latitudes. From there it propagates approximately radially away from the Sun. Setting aside Coronal Mass Ejections (CMEs, Gosling et al., 1974), the solar wind carries with it "open" magnetic field lines that on one end are anchored in the solar photosphere. Along with the solar wind, this open flux fills the heliosphere and is referred to as the heliospheric magnetic field (HMF). As the quiet-time solar wind propagates radially outward with near-constant velocity, the effect of solar rotation distorts the magnetic field into the geometry of an Archimedean spiral, as predicted by Parker (1958). Individual magnetic field lines connect streamlines, packets of solar wind emanating from the same source location on the Sun (or the source surface), and as the Sun rotates so does this source location, which causes the distortion into spiral geometry.

Mariner 2 confirmed the discovery of the solar wind by Lunik-1, and another discovery, that of the persistent interplanetary magnetic field (IMF, Coleman et al., 1960) as predicted by Parker. The observed solar wind speeds also match the prediction by Parker (1958).

In addition, Mariner 2 provided measurements that reveal the IMF sector structure near the ecliptic plane. The cause of the sector structure is the apparent tilt of the solar magnetic axis with

respect to the solar rotation axis. The current sheet separates the regions of outward- and inward-pointing heliospheric magnetic field. Typically, it is so wavy that spacecraft near the plane of the ecliptic, where all major planets are located, would sample both magnetic polarities within one solar rotation period. The Mariner observations clearly associate the HMF with the solar rotation period, although ultimately this confirmation was made with IMP-1 observations a year later (Ness and Wilcox, 1964; see also Ness and Burlaga, 2001).

The (initial) opening angle of the HMF spiral depends on two factors: solar rotation speed and radial speed of the solar wind. Essentially two different solar wind speed regimes have been observed:

1. Fast solar wind: The measured wind speed in the fast solar wind regime is typically ~ 800 km/s, and the freeze-in temperature reflects that of the coronal base (Geiss et al., 1995), which is close to 10^6 K. The areas emitting the fast solar wind can be associated with dark areas, coronal holes, in images of the Sun, e.g., in X-rays (Krieger et al., 1973; Zirker, 1977; Nolte et al., 1977) and in the light of Fe XII (Veronig et al., 2006).
2. Slow solar wind: The typical wind speed in the ecliptic plane varies around ~ 400 km/s (Neugebauer and Synder, 1966; McGregor et al., 2011), and the freeze-in temperature falls within $(1.5\text{--}2) \times 10^6$ K.

The existence of two solar wind regimes will lead to interactions between the magnetized plasmas that have relevant effects on our study. Coronal holes, which are usually found in the Sun's polar regions, can extend to the heliographic equator or even beyond. The fast solar wind from such a coronal hole rotates with approximately the solar sidereal rotation period (Wang and Sheeley, 1993), and emanates from the same heliospheric latitude on the source surface as the slow solar wind outside the coronal hole. A stationary observer close to the Sun will, thus, note recurrent fast and slow solar wind streams. If (1) the pressure gradient becomes sufficiently strong and (2) the speed difference exceeds the local magnetosonic speed, shocks can form. This happens typically at a distance of ≥ 1.5 AU (Richardson et al., 1993). Because these shocks are moving quasi-radially outward, and the magnetic field follows the Parker spiral, the shocks are quasi-perpendicular. An observer close to the ecliptic plane at such distances (2–6 AU) will measure (1) a forward shock, which is moving through the slow wind ahead, accelerating the slow plasma, (2) a stream interface, which is the surface separating two solar wind streams, and (3) a reverse shock, which is moving backwards through the fast wind stream slowing the fast plasma down. If the structure is stable for several rotations, this interaction region can repeatedly be observed in space and is, therefore, called a corotating interaction region (CIR). These go along also with systematic deflections of the solar wind out of the radial direction.

In addition to quasi-periodic CIR phenomena, there are magnetic structures forming as a consequence of irregular events related to solar activity. On short time-scales the latter manifests in the sudden ejection of plasma and magnetic field from the solar corona into the heliosphere. These so-called coronal mass ejections (CMEs) are characterized by velocities of ~ 200 to beyond 3000 km/s and significantly distort the ambient solar wind plasma and magnetic field, including the formation of shocks. CME occurrence rate is closely linked with solar activity level and the number of sunspots, with a higher occurrence rate during the solar maximum. For a review on CMEs see e.g. Chen et al. (2011). A subset of CMEs carries magnetic clouds (MCs), which share a set of common features (Burlaga, 1995), namely an increased magnetic field strength, a slow rotation of the magnetic field direction,

and a low proton temperature. They have a direct effect on the propagation of cosmic rays. An overview of MCs and their relation to CMEs was provided by Démoulin (2008).

The range of solar wind speeds encountered at any given heliographic latitude can be large (McComas et al., 1998), which can lead to the discussed CIR-related effects of compression and deflection. On the backside of CIRs, corotating rarefaction regions (CRRs) form in which fast wind leaves following slower wind behind, forming a region of low density and magnetic field strength.

Fast CMEs can reach speeds of up to several thousand km/s close to the Sun and can drive shock waves through the interplanetary medium ahead. It is also known that CMEs can carry magnetic clouds away from the Sun. Thinned-out regions also form in the wake of fast CMEs. Generally, CMEs and CIRs lead to deviations of the IMF from the ideal Archimedean spiral. Plasma interactions and field structure can now be simulated with heliospheric models.

Important modifications have been made to the Parker magnetic field picture in attempts to quantify cosmic ray motion in an irregular magnetic field (Jokipii, 1966; Jokipii and Parker, 1969) and in response to magnetic field observations of Pioneer 10 and 11 (Smith and Wolfe, 1979) in CRRs that show significant deviations from the Parker spiral in the heliosphere beyond 4 AU. Subsequent studies (Posner, 1999; Posner et al., 2001; Schwadron, 2002; Murphy et al., 2002; Smith, 2013) relate the systematic underwinding near the solar wind stream interface to the dynamic effect on the heliosphere of differential rotation of the photosphere (Fisk, 1996) provided a rather fixed rotation of the coronal structure (Wang and Sheeley, 1993). We will qualitatively discuss the effects of field-line random walk (FLRW) and systematically underwound magnetic field (SUMF) on the HP effect.

1.3. Cosmic rays: modulation in the inner heliosphere

The heliosphere is penetrated by cosmic rays, energetic particles of solar, Jovian, Galactic, and extragalactic origin. Before the dawn of the space age, Forbush (1937) identified sudden decreases, now referred to as Forbush decreases (FDs) in cosmic ray intensity that are linked with geomagnetic activity. Forbush analyzed variations in cosmic ray intensity with a network of ground-based instruments. They are characterized by a sudden onset, a short decrease period, and then a much longer recovery phase. We now understand that FDs are caused by CMEs and magnetic clouds. According to Cane (2000), a close correlation exists between the properties of FDs and the characteristics and the origin of the associated CMEs on the Sun.

So-called 27-day recurrent cosmic ray variations (Forbush, 1954) have been observed that link the cosmic ray flux to the solar rotation period. These sudden short-term decreases in the GCR counting rate have durations of a few days and a magnitude larger than the Earth's daily GCR counting rate variation. Burlaga et al. (1991) found that over large distances in the heliosphere, the GCR intensity and the magnetic field magnitude are anti-correlated.

On time-scales of a few years, cosmic ray transport is determined by the solar activity cycle and the polarity of the solar magnetic field (denoted as $A > 0$ and $A < 0$), e.g. due to gradient and curvature drift. On shorter time-scales it reflects occurrence and properties of heliospheric magnetic field structures (see e.g., Sternal et al., 2011, and references therein). The effects of CIRs on GCR transport were first studied about 35 years ago (Barnes and Simpson, 1976).

The three-dimensional extent of CIRs and their importance in structuring the quiet heliosphere first became obvious from Ulysses observations at high heliolatitudes. A major surprise of this mission was the observation of pronounced recurrent cosmic ray decreases (RCRDs) up to polar regions (Kunow et al., 1995,

McKibben et al., 1995). Previously it had been presumed that strong 26-day variations would disappear as the spacecraft climbed to higher latitudes (cf., e.g., Dunzlaff et al., 2008). Zhang (1997) and Paizis et al. (1999) studied the amplitude evolution of these RCRDs and their rigidity dependence. They showed that the amplitude has its maximum value around 25–30° and decreases for both lower as well as higher latitudes, which can be explained as a combined effect of the interaction efficiency at low latitudes and a magnetic connection between low and high latitude regions. Zhang (1997) found a linear relation between the rigidity dependence of the latitude variation of the cosmic ray protons and their 26-day variation amplitude. Paizis et al. (1999) could show that adiabatic deceleration can satisfactorily account for this observation. As pointed out by Kota and Jokipii (2001), recurrent modulation may differ for positively and negatively charged particles. This has been investigated by Richardson et al. (1996), who found that recurrent cosmic ray decreases observed close to Earth are much more pronounced in an $A > 0$ than in an $A < 0$ solar magnetic epoch. Kota and Jokipii (1995) and recently Wawrzynczak et al. (2011) modeled RCRDs due to the occurrence of CIRs. They found that both the convection due to the solar wind speed increase and an enhanced diffusion due to higher magnetic field strengths are responsible for the occurrence of RCRDs.

The large-scale global structure of the inner heliosphere that influences GCR modulation can now be predicted by the Wang-Sheeley-Arge (WSA)-ENLIL-Cone modeling system (Odstrčil et al., 2004). The system enables predictive simulations (i.e., the simulations compute faster than events unfold) of corotating and transient heliospheric disturbances. Note that SUMFs are not included in this model. This “hybrid” system does not simulate the origin of CMEs but uses coronagraphic observations, in particular fits of geometric/kinematic parameters, and launches CME-like structures into the solar wind. These structures are computed using the WSA coronal model (Odstrčil and Pizzo, 1999; Falkenberg et al., 2011), which is driven by solar magnetic field observations. This modeling system is implemented at the NASA-based multi-agency Community Coordinated Modeling Center (CCMC) to provide a Run-on-Request service to the community, and it is the first numerical model transitioned into operations at NOAA's Space Weather Prediction Center (SWPC) and runs faster-than-real-time at the NASA's Space Weather Research Center (SWRC). The WSA-ENLIL-Cone model provides us with magnetic field connections across the inner heliosphere. With respect to the HP effect, these modeled connections can be directly compared with the much simpler calculations of connection distances assuming ideal Archimedean spiral field lines.

Section 2 describes, based on several examples and using simplifying assumptions, where and to what extent the HP effect occurs. Section 3 describes the observational inputs used in this work. Section 4 demonstrates the HP effect on observations by the example of GCR variations during the transfer of the Mars Science Laboratory to Mars in late 2011 and early 2012. It also discusses scientific challenges and opportunities associated with the HP effect.

2. The Hohmann–Parker effect: where does it apply to planetary transfers?

What we refer to as the HP effect is the finding that spacecraft on outbound and inbound minimum-energy transfer orbits stay magnetically connected within a small angular distance with its origin planet or its destination planet. We will discuss here the outbound and the inbound cases for Earth and Mars. We also discuss transfers between Mercury and Venus, Venus and Earth, and discuss the systematic characteristics.

2.1. Earth to Mars

The outbound case is shown in Fig. 1. The top panel shows a view of an idealized planetary transfer from Earth to Mars. The counterclockwise motions of Earth and Mars, here on circular orbits (blue and red, respectively) with average distances matching those of the planets and zero inclinations, are provided over the time period of the Hohmann transfer from Earth to Mars, which takes approximately 258 days. The Hohmann transfer orbit is drawn in green. It touches Earth orbit at the beginning of the transfer, and Mars orbit at arrival. Tick marks indicate positions in 40-day intervals. Also drawn are idealized Parker magnetic field lines for 400 km/s constant-speed solar wind, which is a good proxy for average solar wind conditions near the ecliptic plane. These sample field lines are chosen to connect with the Earth environment at 40-day intervals. The bottom panel shows the longitudinal angular magnetic connection distance of the Parker spiral field line separating the TV from the Earth and separating the TV from Mars for three common solar wind speeds (see Fig. 1 in McGregor et al., 2011), 300 (red), 400 (black), and 500 km/s (blue), over time. The lines starting out at the origin on day 0 are the Earth-TV ICD magnetic longitude separations. Those converging at 0° at arrival are the TV-Mars OCD separations. Positive values refer to a magnetic connection westward on the Sun of the relatively outer location.

The ICD grows slightly in the early phase of the transfer orbit. At this time, the TV has a higher angular rotation speed than Earth due to extra kinetic energy that will be transferred into potential gravitational energy at the aphelion of the transfer orbit. The Parker spiral outside Earth orbit would always connect with locations lagging Earth, but radial separation between Earth and

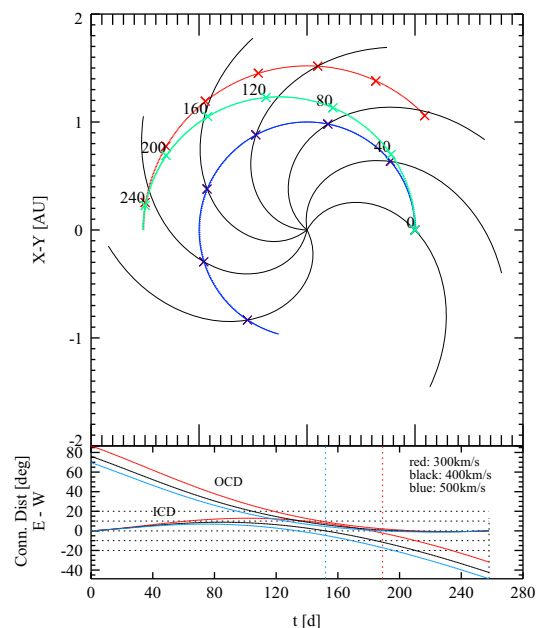


Fig. 1. Earth–Mars Hohmann Transfer. The top panel shows a view of the ecliptic/heliographic plane from the north. The Sun is in the center of the coordinate system. Earth orbit is shown in blue, and that of Mars in red during the transfer of a spacecraft from Earth to Mars (green). Tick marks on the orbits identify constant time intervals (provided in days). The black spirals indicate the 400 km/s solar wind ideal Parker magnetic field lines connecting with the planet of origin. The bottom graph shows the angular magnetic connection distance over time of Earth/TV or ICD, starting at the origin, and TV/Mars or OCD. Positive magnetic connection distance would be an outer location that is magnetically connected to the source surface west of inner location. All magnetic separations are provided for three different solar wind speeds. Vertical dashed lines define the handshake period.

the TV is very small at first. SUMF conditions would improve magnetic connections to Earth in this phase of the transfer. At around day 80, Earth and the TV are radially aligned as the TV slows in angular speed. This is when the ICD reaches its maximum. The magnitude is on the order of 10–15° for very slow solar wind, but under 10° for faster wind speeds or under SUMF conditions. As the Earth catches up swiftly, the ICDs decrease until day 135 for 500 km/s wind or day 190 for 300 km/s wind. At this point, Earth and TV are well aligned along the magnetic field for ~400 km/s solar wind. The angular speed of the TV slows further, so that ICDs quickly grow thereafter. Only around day 200–240 (or 85% of the way), the ICD for very slow wind begins exceeding 10°, however. At arrival, the maximum ICD would reach 30° (slow wind) to 50° (fast wind) or more under SUMF conditions.

The OCD starts out at around 90° due to the TV lagging behind Mars in its orbit. The higher angular speed of the TV decreases this angular separation rapidly, and by day 150 (blue dashed line) – 190 (red dashed line) the OCDs reach smaller values than the ICDs. We will refer to this transition as the “handshake.” The exact time of the handshake is to a certain degree dependent on the speed of the solar wind, as we will show in Section 4, so in a realistic scenario one should refer to a handshake time period. Presence of SUMFs would mimic fast-wind situations and move the handshake to earlier times.

At the time of the handshake, the angular speed of the TV still exceeds that of Mars, so alignment is reached on or slightly after day 200, and a shallow OCD maximum is reached around day 220. The OCD value here is on the order of 2° and, with Mars having higher orbital velocity decreases to zero again by the time of arrival.

In terms of maximum angular magnetic separation from both planets at once, we find 13° for slow wind between days 80 and 120. For higher wind speeds or SUMF conditions, this maximum magnetic separation becomes smaller. In the 400 and 500 km/s speed range the maximum separation distances are well under 10° (~5° for 500 km/s).

The eccentricity of Mars does not significantly change these values. For a transfer orbit to Mars' aphelion, the overall travel time increases to 276 days (from 258). The angular magnetic separation maximum increases to ~15° vs. 13° for the average distance due to the higher kinetic energy needed to reach Mars aphelion, meaning that the TV will move farther ahead in its orbit with respect to Earth in the early phase of the transit. More favorable magnetic connection distances are reached in a transfer to Mars' perihelion, which would take 240 days. The maximum angular magnetic separation from either planet is 11°, again for slow solar wind.

2.2. Mars to Earth

Fig. 2 shows the trajectories of Earth, Mars and the TV on the inbound Hohmann transfer. The inbound Hohmann transfer is initiated by slowing down the angular momentum of the TV. In turn, the TV falls behind Mars, i.e. Mars would be magnetically connected west of MSL on the Sun. This situation prevails during more than half of the transfer period. The OCD achieved here remains rather small, though, with a maximum of ~12° to 22°. Magnetic separation is largest for the slowest solar wind scenario, around day 163, which coincides with the beginning of the rather brief handshake period (days 163–174). Then the destination planet, Earth, rapidly establishes a better magnetic connection for all wind speeds. Interestingly, around the day of arrival there would be a magnetic connection established between the planets of origin and destination if the solar wind speed is around 300 km/s. This is caused by the TV catching up to Mars again with its increased angular velocity close to the Hohmann orbit perihelion.

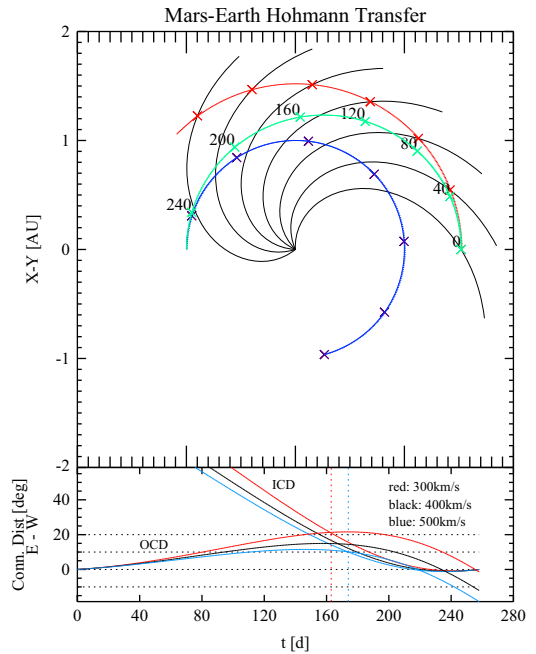


Fig. 2. Mars–Earth Hohmann Transfer. Same views as Fig. 1, but for an inbound transfer from Mars to Earth.

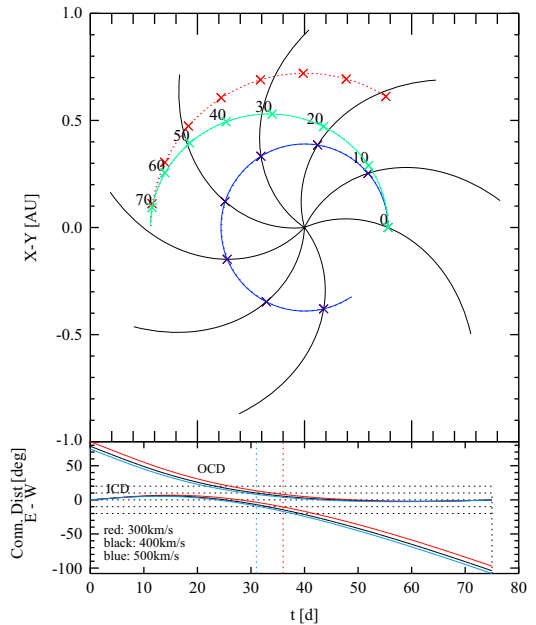


Fig. 3. Mercury–Venus Hohmann Transfer. Same views as Fig. 1, but for an outbound transfer from Mercury, blue orbit, to Venus, red orbit.

Similar to the outbound scenario, a transfer from Mars' perihelion (aphelion) would lead to smaller (larger) connection distances.

2.3. Mercury–Venus and Venus–Earth

The scenarios for Mercury–Venus (Fig. 3) and Venus–Earth (Fig. 4) transits are qualitatively very similar to that of the Earth–Mars transit except that maximum magnetic connection distances are smaller. They are ~10° for Mercury–Venus and ~7° for Venus–Earth outbound transits. The main systematic difference between the outer and inner planet scenarios is the non-radial magnetic field component of

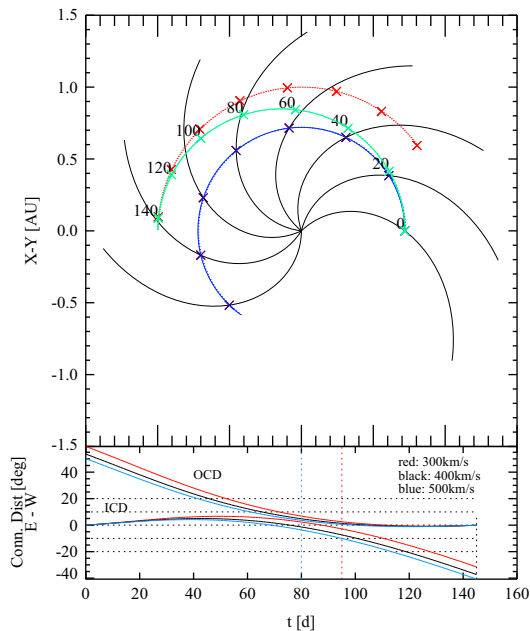


Fig. 4. Venus–Earth Hohmann Transfer. Same views as Fig. 1, but for an outbound transfer from Venus, blue orbit, to Earth, red orbit.

the nominal Parker spiral, which strongly increases with radius (but less strongly under SUMF conditions). As discussed above for the outbound transfer, at the outset the TV has a higher angular orbital speed than the inner planet, which leads to “racing west” of the Parker spiral that magnetically connects the TV with the Sun. This reverses later when the TV falls behind the host planet magnetic connection. The more non-radial the Parker field is, the more weight falls on the initial racing west, as the magnetic field connects with heliospheric locations farther ahead of the planet of origin. This is why the Parker separation is largest for the Earth–Mars transit during the early phase, in particular for slow solar wind speeds, which exacerbate the trend.

“Falling behind” of the TV in the later stage is more important for a transit from a planet inside Earth orbit, say Mercury–Venus, where the magnetic field is more radial between these two orbits than between Earth and Mars orbit. Accordingly, higher solar wind speeds and SUMF conditions tend to increase maximum magnetic connection distances of the TV with the planet of origin and of destination in the later phase of the transfer, but a very small absolute value of the magnetic connection distance with the arrival planet persists.

Also noteworthy is when, relative to the total transfer period, the “handshake” takes place between the origin and the destination planet. This is influenced by the ratio of the semimajor axes of outer and inner planet. A large ratio tends to drive the handshake to an earlier transfer phase. For the Mercury–Venus case, in which the semimajor axis ratio outer to inner planet is $S_{rel}=1.85$, the handshake period happens before the mid-point of the transfer. The Venus–Earth ($S_{rel}=1.39$) and Earth–Mars ($S_{rel}=1.52$) handshake periods are centered around the 2/3 mark. The Venus–Earth handshake happens slightly earlier than that of the Earth–Mars transit. We discussed the effect of eccentricity above in terms of the maximum magnetic connection distances for the Earth–Mars transit. The trends found there also apply to the inner planet transfers. Similarly, the locations of the handshake periods are influenced by eccentricity. An outbound transfer from an inner planet at aphelion would be similar to a scenario with circular orbits that have a slightly smaller S_{rel} , which would lead to a rather late handshake, and vice versa.

2.4. Venus–Mercury and Earth–Venus

The Venus–Mercury and Earth–Venus examples (not shown) both have as the lowest maximum magnetic separation, $\sim 13^\circ$, for an inbound transfer. This value in both cases is achieved before the inbound handshake, whereas for the Mars-to-Earth case it coincides with the handshake. All inbound handshake periods happen rather late, near the 2/3 mark of the transfer period. For all inbound transfers, a (longitudinal) magnetic field alignment of the TV with the outer planet happens after the handshake close to or at arrival. The dominant magnetic connection during inbound transfers therefore is with the planet of origin. This is mostly the case for outbound transfers (with the exception of the Mercury–Venus transfer) as well, but much less pronounced.

3. Observations and models

3.1. MSL/RAD

The Radiation Assessment Detector (RAD, Hassler et al., 2012) builds on the HETn concept (Posner et al., 2005). It was originally designed for inner-heliospheric missions with the purpose to measure cosmic rays and solar energetic particles (SEPs) and solar neutrons and has been refitted as a radiation monitor intended for the surface of Mars. It combines a solid-state detector stack with a CsI calorimeter. Anti-coincidence and plastic detector allow for neutron detection. During the cruise phase, RAD was embedded in the Curiosity rover, but also shielded by the heat shield and back shell, descent stage and propellant needed for landing, and the MSL cruise stage. We use the plastic detector count rate in dosimetry mode as cosmic ray proxy.

3.2. SOHO/COSTEP-EPHIN

The Electron Proton Helium Instrument (EPHIN) is part of the Comprehensive Suprathermal and Energetic Particle Analyzer (COSTEP) (Müller-Mellin et al., 1995). In orbit since 1995, the Solar and Heliospheric Observatory (SOHO) is located near the L1 Lagrangian point of the Sun–Earth–Moon system. COSTEP-EPHIN consists of six solid-state detectors (SSDs) stacked within active anticoincidence shielding. The instrument is sensitive to particles of the minimum-ionizing range, including galactic cosmic ray protons. The stopping power from the active detectors sets the energy ranges for full particle analysis by using the multiple dE/dx method (McDonald and Ludwig, 1964) for relativistic electrons as 150 keV–10 MeV and energetic ions (p, He) as 4 MeV/n to > 54 MeV/n. We utilize as a proxy for GCRs the COSTEP-EPHIN F detector data count rates with minimum proton energies of 54 MeV.

3.3. Mars Odyssey and Mars Express/ASPERA

At the time of the transfer of MSL to Mars, there were no dedicated primary cosmic ray detectors in operation at Mars. However, there were instruments on Mars Odyssey and Mars Express that provide proxy data on GCRs that are very useful for this study.

3.3.1. Mars Odyssey/GRS-HEND

Mars Odyssey carries the Gamma Ray Spectrometer suite, consisting of three subsystems, the gamma ray detector, the Neutron Spectrometer (NS), and the High Energy Neutron Detector (HEND) (Boynton et al., 2004). The HEND itself consists of five sensors, covering various ranges of neutron energies. The Gamma Ray Spectrometer suite, including HEND and the Neutron Spectrometer (NS), are designed to measure secondary particles produced by the interactions

of primary energetic GCR and solar particles; the instruments therefore indirectly measure the local energetic particle environment. Zeitlin et al. (2010) analyzed the responses of the three instruments to SEPs and GCRs. Here we use the SCIH (scintillator inner-high) count rates as our GCR proxy for Mars.

3.3.2. Mars Express/ASPERA

The Mars Express spacecraft was designed to examine the water cycle on Mars (Chicarro et al., 2004). Among its complement of instrumentation is the Analyzer of Space Plasmas and Energetic Atoms (ASPERA-3) experiment (Barabash et al., 2004, 2006). In this paper we construct an instrument background from the ASPERA-3 Electron Spectrometer (ELS) which we use as a proxy of GCR activity. The electron plasma signal from Mars is mostly observed below 10 keV by ELS. Thus, counts above 10 keV are accumulated in an interval of 25 min and adjusted by determining the fraction of the volume of space blocked by Mars from orbital positions of the planet relative to the spacecraft in 10 s intervals.

3.4. STEREO A and STEREO B HET

The High-Energy Telescopes (HET, von Rosenvinge et al., 2008) are energetic particle sensors contributing to the In Situ Measurements of Particles and CME Transients (IMPACT, Luhmann et al., 2008) investigation onboard the twin Solar Terrestrial Relations Observatory (STEREO, Kaiser et al., 2008) mission spacecraft. The HETs provide the highest-energy particle measurements on STEREO, ranging from ~ 13 to beyond 100 MeV for protons. We use the HET proton channel of 60–100 MeV during the cruise phase of MSL to Mars, which outside SEP periods is dominated by GCRs. It has limited statistics, though, due to the limitation in view to the acceptance cone as defined by the HET detector stack. In the absence of anisotropy, the measurements (in flux units) are representative of GCR fluxes.

At MSL launch, STEREO A/B was at 0.97/1.08 AU distance from the Sun, approximately $106^\circ/106^\circ$ ahead/behind of Earth in its orbit. At the end of the transfer period, STEREO A/B was at 0.97/1.03 AU distance from the Sun, approximately $122^\circ/115^\circ$ ahead/behind of Earth in its orbit. Whereas Earth heliographic latitude changed from 2° to 6° , STEREO A/B changed from $-5^\circ/2^\circ$ to $0^\circ/-6^\circ$ heliographic latitude.

3.5. WSA-ENLIL solar wind modeling with GONG inputs

The WSA-ENLIL coupled model sets the magnetic field values at the solar surface using synoptic photospheric magnetograms. Synoptic magnetograms are maps of the normal magnetic flux at the global photospheric surface. They are constructed by combining full disk magnetograms obtained over a full solar rotation with a weighting function applied to each magnetogram which strongly favors data taken near disk center. The model runs discussed in this paper used synoptic magnetograms provided by the Global Oscillations Network Group (GONG). GONG (<http://gong.nso.edu/data/magmap>) uses full disk magnetograms from six observatories around the world to construct its synoptic magnetograms. These magnetic field maps are updated every hour. We modeled the solar wind with the WSA-ENLIL model at a selection of 364 different times during the transit of MSL from Earth to Mars, using the most recently published map at the time of each model run.

GONG synoptic maps have 1° resolution in the longitudinal direction and 180 pixels evenly spaced in the sine of the latitude. The WSA component of the coupled model translates the input magnetogram onto its own internal grid which has a 2.5° spacing in both latitude and longitude.

This sets the lower limit on the scale of features which can be accurately reproduced in our model solutions. In reality, however,

the model inaccuracies are dominated by the model's use of a potential field approximation in the low corona and by its use of synoptic magnetograms which introduces the assumption that the global solar field has not changed significantly during the preceding rotation period. These are both over-simplifications. Validation studies (MacNeice, 2009; MacNeice et al., 2011) have shown that field lines traced from the inner planets to the solar surface have average errors in the location of their photospheric footpoints on the order of $20\text{--}30^\circ$, and that the model estimates for the arrival times of high speed streams and sector boundary crossings at L1 have similar errors.

4. Hohmann–Parker effect by the example of the Mars science laboratory transfer from Earth to Mars

4.1. Observations-driven simulation of longitudinal magnetic connection distances and their variability

For our analysis, almost the entire MSL transfer period, November 26, 2011–August 6, 2012, has been modeled with WSA-ENLIL driven by GONG observations. The simulations generated magnetic connections between the inner boundary of the model at 21.5 solar radii and the locations of Earth, MSL, and Mars in the heliosphere. The coordinates of the modeled magnetic foot points have been used to determine the longitude and latitude connection distances between MSL and Earth/Mars. We assume that magnetic field geometry between the inner model boundary and the source surface further down is radial to the first order.

The top three panels of Fig. 5 show simulated magnetic connection distances of Earth and Mars from MSL during the transfer period. The top panel shows ICDs and OCDs, the second panel magnetic latitude

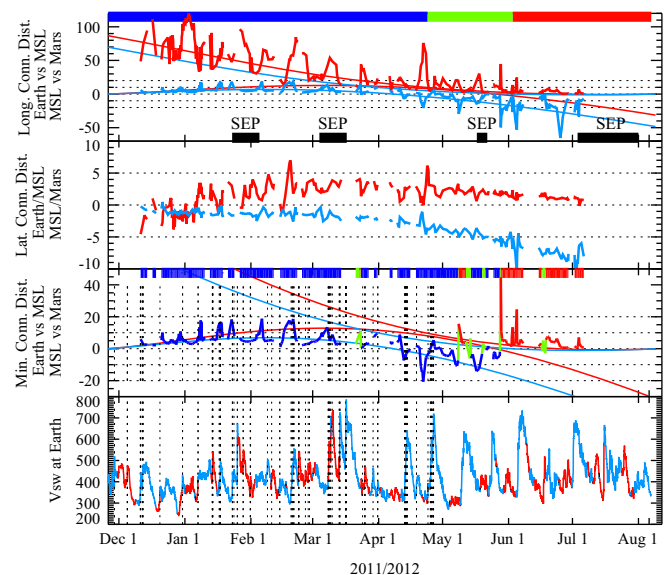


Fig. 5. Earth-MSL-Mars Simulated Magnetic Connection Distances. The top three panels show WSA-ENLIL generated magnetic connection distances from MSL on its way to Mars. The top graph displays the ICD (blue) and OCD (red) in longitude at the source surface. Accordingly, the second graph shows the latitude equivalent of ICD and OCD. The third graph shows the minimum magnetic connection distance, either taken from ICD, blue, OCD, red, or, if the minimum switches in an interval, in green. The smooth curves indicate our predictions under the assumptions of Parker field with constant solar wind speed for 300 km/s (red) or 500 km/s (blue) as shown in Fig. 1. Horizontal bars indicate the preferred (i.e., smaller) magnetic separation from Fig. 1 (top graph) and from simulations (third graph). The bottom panel shows actual solar wind speeds as measured at Earth by ACE and Wind. Colors indicate polarity of the IMF (inward – blue and outward – red) and vertical dashed lines highlight steep speed gradients.

connection distances, with the latitude equivalents of OCD (MSL–Mars) in red and ICD (Earth–MSL) in blue. The third panel on the other hand selects the minimum magnetic connection distance of MSL from the two planets. The colors are indicators of the minimum magnetic connection distance. In addition to Earth/blue and Mars/red, a switch from planet to planet in minimum magnetic connection distance is highlighted in green. The smooth envelope guiding the curves in the top and third panels shows our simplified predictions for the magnetic connection distance assuming constant ~ 300 (red) or ~ 500 km/s (blue) solar wind. The expected preferred magnetic connections and handshake period (green) are indicated in the horizontal bar on top.

In comparison, transitions between the planets as shown in our simulation occur near and during the predicted handshake period (compare horizontal bars of top and third panel). We observe that the more realistic transition period, i.e. the period of overlapping color range, is about twice as wide as the one assuming constant-speed solar wind.

We find that the observations-driven simulation of magnetic connection distances generally is in agreement with the theoretical prediction of the HP effect. The averages of magnetic connection distances are well within the theoretical prediction of the 300–500 km/s (constant) solar wind speed range.

However, we observe occurrences in which the HP effect breaks down in excursions that for brief periods of time maintain magnetic connection distances that are large or at least exceed the predicted range. In order to determine the cause for the excursions beyond our prediction, we show the observed solar wind speed at Earth in the bottom panel. Note that there are no solar wind observations from the locations of MSL or Mars. The solar wind observations are color coded with the magnetic sector structure, blue indicating inward pointing magnetic field associated predominantly with the northern solar hemisphere and red outward IMF of the southern solar hemisphere during this $A < 0$ solar magnetic cycle.

Our simplified transfer scenario assumes solar wind speeds of 300–500 km/s. Comparison with observations shows that although for most of the time the solar wind speed is within this range, there are periods of very fast and very slow solar wind that exceed the range. The fastest speeds are observed in March and May during the SEP periods and they are related to transient, CME-related solar wind that is not modeled in our simulations. Other fast periods are present in the May through July time frame and these recur with the frequency of solar rotation. These fast streams originate in long-lived equatorial coronal hole extensions and form CIRs.

The effect of solar wind speed gradients and SUMFs, as compared to different overall levels of constant solar wind speed, has not been included in our idealized treatment of the HP effect. In the bottom panels of Fig. 5 we added vertical lines that indicate positive speed gradients exceeding 50 km/s within 24 h. There is a good correspondence of these speed gradient indicators with some of the (upward) excursions of the Earth–MSL magnetic connection distance simulation. The brief upward excursions of the ICD occur systematically during the December through April time period. Upward excursions refer to periods during which the location at the larger radial distance (MSL) is magnetically connected farther west on the sun than the inner location (Earth). As we described in Section 2.1, during the early transfer phase MSL moves west (ahead) of Earth and in its magnetic connection to the Sun. However, corotating fronts approach the Earth/MSL system from the east (behind). This leads to Earth seeing any corotating fast streams earlier than MSL. Therefore, while Earth is embedded in the leading edge of a fast stream, MSL will still be located in the tail end of a slow-stream region. During this phase, the foot point of the Earth-connected magnetic field line moves closer to the central meridian of the Sun as viewed from Earth, while MSL's magnetic connection remains nearly steady. Therefore, the ICD

increases sharply in the sense that it reaches higher positive values. The durations of each individual excursion are brief, ending when MSL encounters the fast stream itself. Generally, the larger the average westward magnetic connection distance of MSL vs. Earth is, say, for constant ~ 400 km/s solar wind speed, the longer the periods of these speed-gradient excursions would last. At the time of overtaking, meaning MSL crosses the Earth-locked 400 km/s field line eastward, the upward excursions of the ICD should disappear. And this is reflected in the simulation output, with its last upward excursion seen in late February 2012. After this period, analogous downward ICD excursions begin, which are a sign of MSL first encountering CIR fast streams and Earth temporarily being magnetically connected (far) west of MSL.

Qualitatively, the speed gradient effect also explains systematic upward excursions of the OCD. During the entire cruise phase, MSL “observes” CIR fast streams before they reach Mars. Therefore, the MSL magnetic footpoint moves eastward during fast stream encounter, whereas Mars remains in slow wind. The westward magnetic connection distance increases, resulting in a temporary upward excursion of the OCD. Only at arrival, MSL reaches the Mars-locked 400 km/s field line, but never crosses it eastward.

Limiting the discussion to the third panel of Fig. 5, magnetic connection distances from MSL to the better-connected planet, the cumulative duration of the excursions is rather limited. Solar wind speed longitudinal gradients can lead to higher maximum magnetic connection distances than predicted based on the constant-speed assumption. While the duration of the encounter of the leading edge of a fast solar wind stream can be long (small gradient), the duration of an excursion is determined by corotation delay between MSL and the (better connected) planet. For the Earth-to-Mars transfer, corotation delay during any phase of the transfer is less than a day. Assuming that up to three CIR-related gradients per solar rotation period occur, the worst case scenario would still limit the cumulative duration to $\sim 10\%$ of the portion of the cruise that has the largest minimum magnetic connection distance. Therefore, in the overwhelming majority of the transfer period from Earth to Mars, MSL is within 10° of magnetic connection distance from either Earth or Mars. As our simulation shows, the excursions rarely exceed 20° in longitude. Thus the gradient effect increases the extent of the connection distance envelope by less than a factor of two.

Aspect we did not discuss in detail is the radial dependences of the effects of solar wind stream–stream interactions. The region of the heliopause where SUMF is expected grows with radial distance. Therefore, SUMF effects on magnetic connection distance are expected to be larger and longer lasting for the Earth–Mars and Mars–Earth transits than for those inside Earth orbit. Generally, solar wind speed gradients in CRRs are small, much smaller than in CIRs (see, e.g., the schematic Fig. 1 of Richardson et al., 1993), therefore qualitatively SUMF effects on magnetic connection during transfers are adequately described in our discussion of the constant-speed scenarios in Sections 2.1–2.4.

We expect that CIR-related compression interactions grow in influence with increasing radial distance as more fast wind parcels will catch up with slower wind in their near-radial path. Stream–stream interactions are already known to occur between Mercury and the Sun. Schwenn (1990) shows that solar wind bulk speed gradients decline significantly between 0.29 and 1 AU, from on average $> 100 \text{ km s}^{-1} \text{ deg}^{-1}$ to $< 40 \text{ km s}^{-1} \text{ deg}^{-1}$. Even sharper speed gradients can be expected at or near the solar source surface. Here, also stronger compressions in the magnetic field would occur, enhancing gradient drift effects on GCRs. In order to fully understand and analyze the effect of stream–stream interactions on the HP effect, we would certainly need solar wind information from closer to the Sun than 1 AU during a transfer interval.

4.2. Considerations of the HP latitudinal magnetic separation: challenges and opportunities

Latitudinal magnetic connection distance has not been treated in necessary detail. The inclination of Mars orbit vs. Earth orbit is only 1.8° as they are both closely tied to the Laplace invariable plane of the solar system angular momentum, so there is only a small latitude adjustment out of the ecliptic plane necessary to reach Mars. Note however that both Earth and Mars orbit are more significantly inclined with respect to the heliographic equator, 7.2° and 5.7° respectively. Therefore, their maximum angular separation in heliographic latitude can add up to almost 13° , which is typically reached only during Mars oppositions that occur when Earth reaches heliographic latitude extremes in the late March or late September time frame. During the Hohmann transfer, Earth and Mars are never separated in heliographic longitude by more than 90° , the quadrature separation with respect to the Sun. Therefore, the maximum heliographic latitudinal separation would be limited to $\sim 6.5^\circ$. Magnetic connection distance is influenced by solar wind dynamics and interactions (Pizzo, 1978, 1980) and could in some cases exceed the maximum heliographic latitude separation. Our simulation that includes plasma effects, such as north/southward deflections of the solar wind in CIRs, shows that for the most part the magnetic connection distances between MSL and both planets stay within this envelope. Only the latitude-equivalent of the ICD exceeds this value in July 2012, which occurs after the handshake period. Looking at the preferred connection only, the maximum latitudinal magnetic connection distance is less than 5° . Note, however, that Fisk-type (Fisk, 1996) field effects could still lead to larger latitudinal magnetic separations than shown.

Cosmic ray studies have shown that RCRD are caused by CIRs and that Ulysses has seen that low-latitude CIRs cause RCRDs that extend well beyond the latitudes where fast and slow wind streams interact. Competing theories of field line foot point motion can explain direct magnetic connections between high and low or latitudes (Fisk and Jokipii, 1999) or near-radial longitudes (Schwadron, 2002), which would allow GCRs to propagate easier in latitude or near-radially on one side of the heliospheric current sheet. Utilizing the HP effect, these studies can be pursued further, by including situations in which the effects of CIRs on RCRDs can be analyzed from the perspective of opposite sides of the heliospheric current sheet. Furthermore, studies of SEP composition in connection with the HP effect could shed more light on the acceleration mechanism(s). The persistence of the HP effect increases the likelihood of observing the onset of a SEP event during a period in which two spacecraft are well-connected in solar longitude, but at the same time located on opposing sides of the heliospheric current sheet (HCS). The HCS separates parcels of plasma at the sun that are located closely together on the source surface, but they can be quite far apart in terms of the foot point location in the photosphere, in particular due to the likely presence of closed magnetic field lines in between these foot points. Significant differences in particle intensity or composition could hint at acceleration mechanisms low down in the corona, whereas similarities could hint at a shock acceleration mechanism higher up at or beyond the source surface.

4.3. Comparison of GCR proxy observations during the MSL transfer interval

This section describes and discusses the GCR observations observed at Earth, MSL, and Mars. In order to allow for a comparison with GCRs measured far away from a magnetic connection, we also added STEREO A and B High-Energy Telescope GCR observations. The combination of the GCR observations from vantage points that are connected due to the HP effect (Earth-MSL entire transfer; MSL-Mars

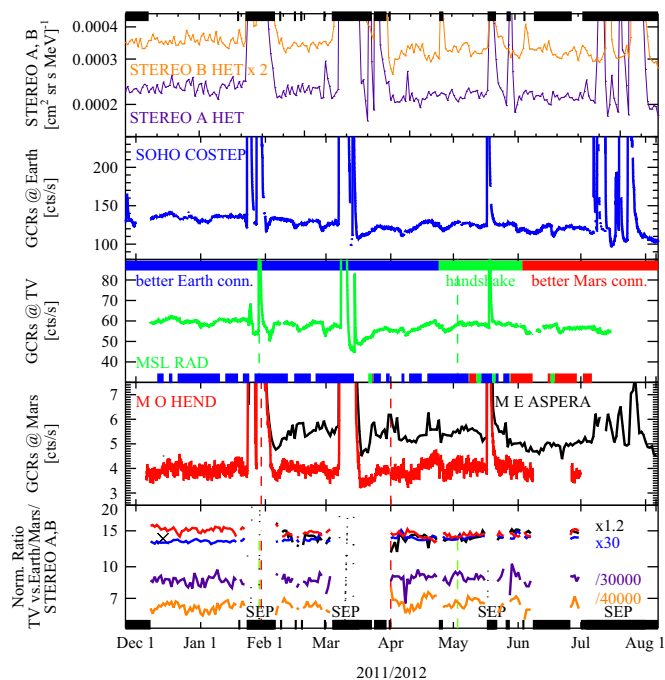


Fig. 6. Cosmic Ray Observations During the MSL Cruise. STEREO A and B (top panel), SOHO/COSTEP (second panel) near Earth, MSL/RAD (third panel) in transfer from Earth to Mars and a combination of Mars Express/ASPERA (black) and Mars Odyssey/HEND (red) cosmic ray proxy observations at Mars (fourth panel) during the planetary transfer of MSL from Earth to Mars in 2011/2012. The third panel also contains indicators of preferred magnetic connection with Earth (blue) and Mars (red) or both (green) from Fig. 1 (top bar) and from Fig. 5 (bottom bar). The bottom panel shows the GCR proxy ratios of the TV (MSL) vs. Earth (SOHO) in blue and TV vs. Mars (Mars Odyssey and MARS Express) in red and black in arbitrary units. Periods with SEPs are highlighted at bottom and excluded in the bottom panel.

late transfer) with those that are not (MSL-STEREO A; MSL-STEREO B) allows us to test our hypothesis of correlated vs. uncorrelated cosmic ray intensities.

The observations are shown in Fig. 6. The commonality between the detectors is that they all are deeply embedded in the spacecraft and instruments, leading to rather high low-energy cut-off values for electrons and ions. Outside of SEP events, the count rates are dominated by high-energy protons and their secondaries from GCRs. The individual low-energy cut-offs are different, however. We estimate that MSL/RAD's (plastic E-detector) cutoff is highest, followed by STEREO A and B 60–100 MeV protons, and by that of SOHO/COSTEP (F detector, > 54 MeV). The Mars-based observations presumably have the lowest cut-offs and see higher SEP count rates (and longer SEP durations) than RAD, HET, and COSTEP. STEREO's HETs and Mars Odyssey's HEND (plastic) detector provide the smallest geometric factors, which leads to the largest statistical uncertainty of 3.2% for HET and 0.8%/day for HEND. For all other detectors, statistical errors are insignificant. The uncertainty of low-energy cut-offs for RAD, HEND and ASPERA, which are dependent on angle of incidence, lead to measurements during solar particle events that are of limited value. SEPs are characterized by onset anisotropies, variable composition of energetic particles (in particular electrons vs. ions), and the particle intensity depends very strongly on the energy interval (or threshold). We therefore exclude the SEP time periods from our discussion of the observations and rather focus on the GCR proton component measured outside SEP periods.

The cruise phase of MSL falls into the detector commissioning window of RAD. The measurements (green, center panel) show gaps in particular in the early phase of the transfer. In addition,

changes in instrument operations had to be compensated for. Periods of operational change are indicated by dashed vertical lines in the RAD panel. We also observed the effects of operational changes with HEND, all of which we attempted to compensate for (see dashed red lines in the 4th panel). Due to the operational changes, in particular with RAD, there is limited confidence in the utility of very early-phase observations of November and early December 2011 and these had to be excluded. However, the operational changes were successful resulting in good measurements thereafter. This can be seen in the following period, December/January, during which contours of the cosmic ray background between MSL and SOHO/COSTEP are highly correlated and of similar magnitude.

Significant data gaps exist in December (HEND) and December/January (ASPERA) and in June/July (HEND). RAD was turned off in July, 3 weeks before the MSL landing on Mars. ASPERA visually fills one of the important periods in June during which HEND was off, but ASPERA data were not used for our correlation analysis due to its susceptibility to lower-energy particles. We only use times for our analysis in which the detectors RAD, COSTEP, HEND, and HET (on both STEREO A and B) provided data and during which SEPs were absent. The black bars at top and bottom of the figure highlight exclusion periods.

As Fig. 5 (bottom) shows, the middle and late phase of the transfer period is characterized by recurrent solar wind streams and by transient coronal mass ejections, whereas the early phase is quiet. Characteristic ~ 25 to 27-day solar rotation period GCR decreases are typically associated with corotating streams. Interestingly, the 1 AU solar wind measurements show that the dominant corotating fast streams are observed in the early May through early July 2012 time frame with presumably two fast streams present per solar rotation. Here the GCR modulation pattern seems irregular. However, the strongest recurrent GCR modulation feature is observed following the March SEP event and might be the result of continuing modulation by the March CME/magnetic cloud for two solar rotations after the original FD. The impact of the March event is clearly visible in the

lowering of the GCR count rate baseline. Smaller such effects are seen after the January event and the May event. The events in July, which included one of the most significant fast CMEs ever measured, also produced a significant drop in GCR count rate as seen by COSTEP.

Our hypothesis is tested in the bottom panel, which provides GCR ratios of various vantage points vs. MSL. We predicted correlated GCR fluxes for almost the entire cruise phase between Earth and MSL, and good correlations during the late phase of the transfer between MSL and Mars, which should result in near-constant ratios (three upper curves in the bottom panel). Uncorrelated GCR observations outside the HP effect should be the result if comparing STEREO A/B vs. MSL, as shown in the bottom two curves. Here we need to note that there is not only a significant angular (and similarly magnetic) longitude separation on the order of 100° , but also a separation in latitudes on the order of $5\text{--}10^\circ$. However, there are no other GCR observations available that would provide us with a longitude-only separation. Taking this caveat into account, the difference is clearly recognizable.

In order to systematically analyze the correlations in these ratios, we included Fig. 7. The correlation coefficients are significantly higher for those ratios that fall in the HP effect than for those outside of it. The correlation coefficient for the entire cruise phase between Earth and MSL is highest, at 0.86 (Fig. 7, top left). Second highest is the correlation coefficient for MSL vs. Mars after the handshake, at 0.72 (top right). Note that gradient and curvature drift allow particles to move across field lines and as such deemphasize the relevance of magnetic connection. As stream-stream interactions of the background (non-CME) solar wind increase and lead to stronger gradients with distance from the sun, gradient drift effects would increase with distance. However, curvature drifts would decrease with distance in response to the larger curvature radius of the Parker spiral with r . In general, drift effects tend to lower the GCR correlations of the HP effect.

Much lower, however, than the GCR correlations under HP effect, are the correlations clearly falling outside the influence of

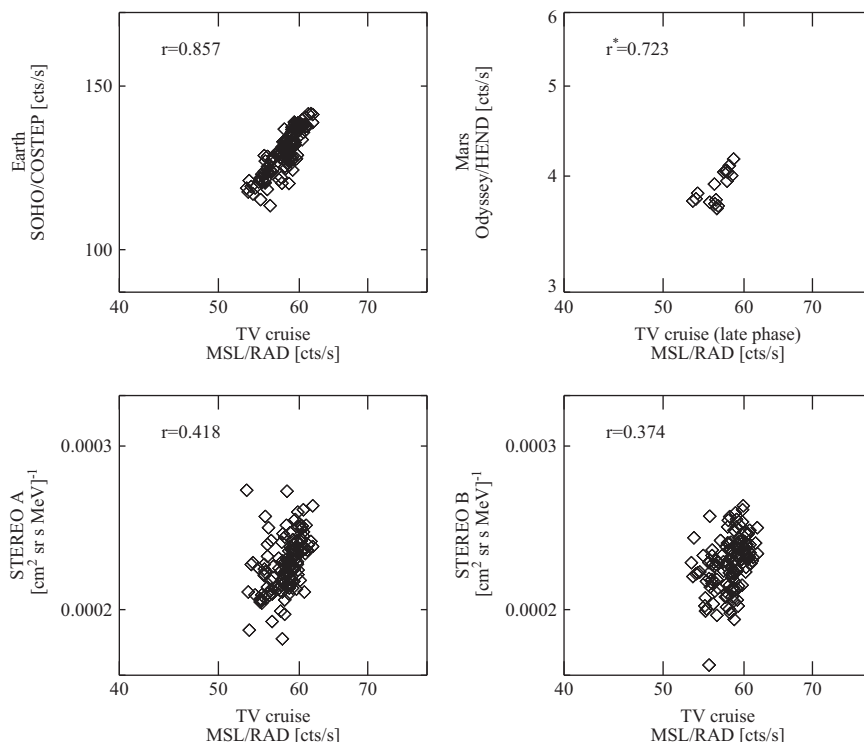


Fig. 7. Hohmann–Parker Effect on GCR Observations. Correlation graphs comparing cosmic ray rates at MSL on the transfer to Mars with Earth (top left) and Mars (late phase after handshake at \sim day 180 only, top right) and STEREO-A (bottom left) and STEREO-B (bottom right). Correlation coefficients of least-square fits are provided.

the HP effect between MSL and STEREO A (0.42, bottom left) and STEREO B (0.37, bottom right) during the entire cruise phase. A small residual correlation is expected, though, for all GCR measurements in the inner heliosphere during the rising phase of solar activity, in which the MSL cruise falls, due to the overall drop of GCR intensity with time. A negative effect on the correlation derives from the relatively larger statistical uncertainty of the STEREO observations, which is only slightly smaller than the modulation signal. However, the modulation pattern is still recognizable in the top panel of Fig. 6, and clearly out of phase with the patterns seen at MSL, at Earth and at Mars. Therefore, we believe that the smaller correlation between both STEREOs and the TV due to the absence of the HP effect is a robust result.

4.4. Hohmann–Parker effect potentially practical and scientific applications

There are practical uses for the HP effect particularly during solar active periods.

For locations along the magnetic field lines connected with those crossing near Earth, early warning of prompt solar energetic particle (SEP) events from the Sun with forecasting systems such as REleASE (Posner, 2007) or UMASEP (Núñez, 2011) in place would be possible. The radiation field in the inner heliosphere would show relativistic electrons and protons racing away from the Sun along well-connected field lines. Within 10 (15) min after release of solar energetic particles from the Sun during a flare/CME event, relativistic electrons and protons would have reached Earth (Mars). At the time, hazardous high-intensity protons (> 10 – 100 MeV) are still within 0.5 AU from the Sun. The fast-moving (test-) particles probe the magnetic field ahead of the protons for instantaneous magnetic connectivity, which would not otherwise be possible. So with a REleASE and/or UMASEP system in place at both ends of the planetary transfer, potential explorers on the way to and back from Mars could be warned in advance of sudden increases in SEPs. By the time the hazardous protons have reached the transfer vehicle, the astronauts could have taken any necessary precautionary measures against this exposure. This warning system could be applied to all neighboring planetary transfers between the orbits of Mercury to Mars, as long as the origin planet and the destination planet have relativistic electron and proton measurement capabilities in place, i.e. at the respective planet–Sun L1 locations.

Despite its relatively low value of $< 5^\circ$, any latitudinal magnetic connection distance can have a significant effect on the longitudinal magnetic separation. Schwenn (1990) found that solar wind speed latitudinal gradients can be large in the ecliptic plane. This situation would allow for latitudinal layers of fast and slow solar wind speed. One layer could embed a planet, the other a TV seemingly co-located in longitude and distance to be magnetically connected at significantly different longitudes at the source surface. Latitudinal speed gradient effects are included in our magnetic (longitude) separation simulations with ENLIL and might add another contribution to the excursions not addressed before. On the other hand, the effect can also bring the magnetic connections of planet and TV closer together at times when they appear to be separated significantly in solar longitude.

Speed, elemental and ionic charge-state composition are inherent properties of the solar wind that can be dramatically different on either side of the stream interface between the fast and slow solar wind (Geiss et al., 1995), in particular on the leading edge of high-speed streams (Posner et al., 2001). The HP effect presumably increases the likelihood of the better-connected planet and the TV both being embedded in solar wind on the one side of a stream interface. Slow solar wind is present on both sides of the solar wind current sheet that separates outward from inward IMF, but it

is not well known whether significant solar wind composition changes occur when comparing wind parcels north and south of the current sheet. This is because periods of field-aligned spacecraft in longitude that at the same time are separated by more than fractions of a degree in latitude do not occur very often. During the transfer to Mars, the latitudinal separation, although $< 5^\circ$, was much larger than the typical latitude separation of spacecraft bound gravitationally to the Earth/moon system (such as ACE and Wind). This would increase the time periods in which solar wind is measured both north and south of the current sheet. Therefore, the (persistent) HP effect would make such studies easier to come by.

The existence of achievable planetary transfer orbits that already closely track magnetic connections with planet-bound locations allows us to speculate about mission scenarios that utilize the HP effect for the benefit of scientific understanding. We have seen that the outbound transfer from Earth to Mars would lead the TV to initially run ahead of its magnetic connection with Earth, whereas after the handshake it would fall behind the Earth-connected field line. We envision a mission scenario of two or even three identically-equipped spacecraft, one of which would be placed at Earth's L1. The second would require the outbound acceleration away from the home planet in a more gradual and more continuous way than that of the minimum-energy transfer orbit, which, depending on payload mass, could be achievable with solar electric and/or solar sail propulsion. This way, the average magnetic connection distance between the two spacecraft could be minimized and better and longer maintained, than otherwise possible. The third spacecraft would be sent along the inbound Hohmann transfer trajectory, also with an adjustment of continuous acceleration in order to minimize magnetic connection distance with Earth's L1. Increasing distances along the magnetic field over the 4–5 months long mission would allow us to learn about particle propagation, including the quantitative determination of cosmic ray gradients and solar energetic particle gradients along the field. In terms of SEP gradients, this would be particularly important, as all other mission scenarios would require chance alignments (even alignment of two spacecraft is unlikely to coincide with an SEP onset) along the magnetic field during the short SEP onset phase, whereas the maintenance of the magnetic connection during a solar active phase would reasonably ensure the observation of several SEP event onsets during the mission, as the MSL/Earth or Mars/MSL examples have shown. Solar wind plasma and composition changes could help us understand processes at the common solar wind source. Solar radio instrumentation could shed light on the generation process of Langmuir waves from the expansion of energetic electrons, and how this generation changes along the magnetic field. A sample payload for each spacecraft thus could include solar wind plasma, magnetic field, and composition instrumentation, comprehensive SEP and GCR spectrometers, and Langmuir probes.

Acknowledgments

RAD team members at Southwest Research Institute are supported by NASA/HEOMD under JPL subcontract #1273039. Work performed by R.A. Frahm was supported through NASA contract NASW-00003. E. Böhm, S. Burmeister, J. Köhler, R. Müller-Mellin, G. Reitz, L. Seimetz, and R.F. Wimmer-Schweingruber are funded by Deutsches Zentrum für Luft- und Raumfahrt as part of its science program and by DLR's Space Administration grant 50QM0501 to the Christian Albrechts Universität (CAU) Kiel. A portion of this research was carried out at the Jet Propulsion Laboratory, California Institute of Technology, under a contract with NASA. The SOHO/EPHIN project is supported under Grant 50

OC 1302 by the German Bundesministerium für Wirtschaft through the Deutsches Zentrum für Luft- und Raumfahrt (DLR). We are grateful to the Mars Odyssey Gamma Ray Spectrometer team for making their data available to this study. We would like to thank J. Mottar for graphics support.

References

- Barabash, S., Lundin, R., Andersson, H., Gimholt, J., Holmström, M., Norberg, O., Yamauchi, M., Asamura, K., Coates, A.J., Linder, D.R., Kataria, D.O., Curtis, C.C., Hsieh, K.C., Sandel, B.R., Fedorov, A., Grigoriev, A., Budnik, E., Grande, M., Carter, M., Reading, D.H., Koskinen, H., Kallio, E., Riihelä, P., Säles, T., Kozyra, J.U., Krupp, N., Livi, S., Woch, J., Luhmann, J.G., McKenna-Lawlor, S., Orsini, S., Cerulli-Lrelli, R., Maggi, M., Morbidini, A., Mura, A., Milillo, A., Roelof, E.C., Williams, D.J., Sauvaud, J.-A., Thocaven, J.-J., Moreau, T., Winningham, J.D., Frahm, R.A., Scherrer, J., Sharber, J.R., Wurz, P., Bochsler, P., 2004. ASPERA-3: Analyser of Space Plasmas and Energetic Ions for Mars Express, in MARS EXPRESS: The Scientific Payload. In: Wilson, A. (Ed.), European Space Agency Publications Division, vol. SP-1240. European Space Research and Technology Centre, Noordwijk, The Netherlands, pp. 121–139.
- Barabash, S., Lundin, R., Andersson, H., Brinkfeldt, K., Grigoriev, A., Gunell, H., Holmström, M., Yamauchi, M., Asamura, K., Bochsler, P., Wurz, P., Cerulli-Lrelli, R., Mura, A., Milillo, A., Maggi, M., Orsini, S., Coates, A.J., Linder, D.R., Kataria, D.O., Curtis, C.C., Hsieh, K.C., Sandel, B.R., Frahm, R.A., Sharber, J.R., Winningham, J.D., Grande, M., Kallio, E., Koskinen, H., Riihelä, P., Schmidt, W., Säles, T., Kozyra, J.U., Krupp, N., Woch, J., Livi, S., Luhmann, J.G., McKenna-Lawlor, S., Roelof, E.C., Williams, D.J., Sauvaud, J.-A., Fedorov, A., Thocaven, J.-J., 2006. The Analyser of Space Plasmas and Energetic Atoms (ASPERA-3) for the Mars Express Mission. *Space Science Reviews* 126, 113–164.
- Barnes, C.W., Simpson, J.A., 1976. Evidence for interplanetary acceleration of nucleons in corotating interaction regions. *Astrophysical Journal Letters* 210, L91–L96.
- Boynton, W.V., Feldman, W.C., Mitrofanov, I.G., Evans, L.G., Reedy, R.C., Squyres, S.W., Starr, R., Trombka, J.J., D'Uston, C., Arnold, J.R., Englert, P.A.J., Metzger, A.E., Wänke, H., Brückner, J., Drake, D.M., Shinohara, C., Fellows, C., Hamara, D.K., Harshman, K., Kerry, K., Turner, C., Ward, M., Barthe, H., Fuller, K.R., Storms, S.A., Thornton, G.W., Longmire, J.L., Litvak, M.L., Ton'chev, A.K., 2004. The Mars Odyssey gamma-ray spectrometer instrument suite. *Space Science Reviews* 110, 37–83, <http://dx.doi.org/10.1023/B:SPAC.0000021007.76126.15>.
- Burlaga, L.F., 1995. Interplanetary Magnetohydrodynamics. International Series on Astronomy and Astrophysics, vol. 3. Oxford University Press, New York. (ISBN13: 978-0-19-508472-6).
- Burlaga, L.F., McDonald, F.B., Ness, N.F., Lazarus, A.J., 1991. Cosmic ray modulation: Voyager 2 observations 1987–1988. *Journal of Geophysical Research* 96, 3789–3799.
- Cane, H.V., 2000. Coronal mass ejections and Forbush decreases. *Space Science Reviews* 93, 55–77, <http://dx.doi.org/10.1023/A:1026532125747>.
- Chen, C., Wang, Y., Shen, C., Ye, P., Zhang, J., Wang, S., 2011. Statistical study of coronal mass ejection source locations: 2. Role of active regions in CME production. *Journal of Geophysical Research* 116, <http://dx.doi.org/10.1029/2011JA016844>. (CitID A12108).
- Chicarro, A., Martin, P., Trautner, R., 2004. The Mars Express Mission: an overview. In: Wilson, A. (Ed.), Mars Express: The Scientific Payload. European Space Agency Publications Division, European Space Research and Technology Centre, Noordwijk, The Netherlands, vol. SP-1240, pp. 121–139.
- Coleman, P.J., Davis, L., Sonnet, C.P., 1960. Steady component of the interplanetary magnetic field: Pioneer V. *Physical Review Letters* 5, 43.
- Decker, R.B., Krimigis, S.A., Roelof, E.C., Hill, M.E., 2012. No meridional plasma flow in the heliosheath transition region. *Nature* 489, 124.
- Démoulin, P., 2008. A review of the quantitative links between CMEs and magnetic clouds. *Annales Geophysicae* 26, 3113–3125, <http://dx.doi.org/10.5194/angeo-26-3113-2008>.
- Dunzlaff, P., Heber, B., Kopp, A., Rother, O., Müller-Mellin, R., Klassen, A., Gómez-Herrero, R., Wimmer-Schweingruber, R.F., 2008. Observations of recurrent cosmic ray decreases during solar cycles 22 and 23. *Annales Geophysicae* 26, 3127–3138, <http://dx.doi.org/10.5194/angeo-26-3127-2008>.
- Falkenberg, T.V., Taktakishvili, A., Pulkkinen, A., Vennerstrom, S., Odstrčil, D., Brain, D., Delory, G., Mitchell, D., 2011. Evaluating predictions of ICME arrival at Earth and Mars. *Space Weather* 9, <http://dx.doi.org/10.1029/2011SW000682>.
- Fisk, L.A., 1996. Motion of footpoints of heliospheric magnetic field lines at the sun: Implications for recurrent energetic particle events at high heliographic latitudes. *Journal of Geophysical Research* 101, 15,547–15,553, <http://dx.doi.org/10.1029/96JA01005>.
- Fisk, L.A., Jokipii, R.R., 1999. Mechanisms for latitudinal transport of energetic particles in the heliosphere. *Space Science Reviews* 89 (1/2), 115–124, <http://dx.doi.org/10.1023/A:1005285003239>.
- Forbush, S.E., 1954. World-wide cosmic ray variations 1937–1952. *Journal of Geophysical Research* 59, 525–542.
- Forbush, S.E., 1937. On the effects in cosmic-ray intensity observed during the recent magnetic storm. *Physical Review* 51 (12), 1108–1109.
- Geiss, J., Gloeckler, G., von Steiger, R., 1995. Origin of the solar wind from composition data. *Space Science Reviews* 72, 49–60, <http://dx.doi.org/10.1007/BF00768753>.
- Goddard, R., 1919. A method of reaching extreme altitudes. *Smithsonian Miscellaneous Collections* 71, 2.
- Gosling, J.T., Hildner, E., McQueen, R.M., Munro, R.H., Poland, A.I., Ross, C.L., 1974. Mass ejections from the Sun: a view from Skylab. *Journal of Geophysical Research* 79, 4581–4587.
- Hassler, D.M., Zeitlin, C., Wimmer-Schweingruber, R.F., Böttcher, S., Martin, C., Andrews, J., Böhm, E., Brinza, D.E., Bullock, M.A., Burmeister, S., Ehresmann, B., Epperly, M., Grinspoon, D., Köhler, J., Kortmann, O., Neal, K., Peterson, J., Posner, A., Rafkin, S., Seimetz, L., Smith, K.D., Tyler, Y., Weigle, E., Reitz, G., Cucinotta, F.A., 2012. The Radiation Assessment Detector (RAD) investigation. *Space Science Reviews* 170, 503–558.
- Hohmann, W., 1925. Die Erreichbarkeit der Himmelskörper. R. Oldenbourg Munich-Berlin (Reprinted as NASA Techn. Transl. F-44, Langley Field, VA, 1960).
- Jokipii, J.R., 1966. Cosmic-ray propagation. I. Charged particles in a random magnetic field. *Astrophysical Journal* 146, 480–487, <http://dx.doi.org/10.1086/148912>.
- Jokipii, J.R., Parker, E.N., 1969. Random walk of magnetic lines of force in astrophysics. *Physical Review Letters* 21, 44, <http://dx.doi.org/10.1103/PhysRevLett.21.44>.
- Kaiser, M.L., Kucera, T.A., Davila, J.A., Cyr, O.C., Guhathakurta, M., Christian, E.R., 2008. The STEREO mission: an introduction. *Space Science Reviews* 136, 5, <http://dx.doi.org/10.1007/s11214-007-9277-0>.
- Kota, J., Jokipii, J.R., 2001. Cosmic ray transport in a heliospheric magnetic field with non-polar coronal holes. *Space Science Reviews* 27, 529–534, [http://dx.doi.org/10.1016/S0273-1177\(01\)00090-4](http://dx.doi.org/10.1016/S0273-1177(01)00090-4).
- Kota, J., Jokipii, J.R., 1995. Corotating variations of cosmic rays near the south heliospheric pole. *Science* 268, 1024–1025, <http://dx.doi.org/10.1126/science.268.5213.1024>.
- Krieger, A.S., Timothy, A.F., Roelof, E.C., 1973. A coronal hole and its identification as the source of a high velocity solar wind stream. *Solar Physics* 29, 505–525, <http://dx.doi.org/10.1007/BF00150828>.
- Kunow, H., Dröge, W., Heber, B., Müller-Mellin, R., Röhrs, K., Sierks, H., Wibberenz, G., Ducros, R., Ferrando, P., Rastoin, C., Raviart, A., Paizis, C., 1995. High-energy cosmic-ray nuclei results on Ulysses: 2. Effects of a recurrent high-speed stream from the southern polar coronal hole. *Space Science Reviews* 72, 397–402, <http://dx.doi.org/10.1007/BF00768811>.
- Luhmann, J.G., Curtis, D.W., Schroeder, P., McCauley, J., Lin, R.P., Larson, D.E., Bale, S. D., Sauvaud, J.-A., Mewaldt, R.A., Cummings, A.C., Stone, E.C., Davis, A.J., Cook, W.R., Kecman, B., Wiedenbeck, M.E., von Roseninge, T.T., Acuña, M.H., Reichenthal, L.S., Shuman, S., Wortman, K.A., Reames, D.V., Müller-Mellin, R., Kunow, H., Mason, G.M., Walpole, P., Korth, A., Sanderson, T.R., Russell, C.T., Gosling, J.T., 2008. STEREO IMPACT investigations, goals, measurements, and data products overview. *Space Science Reviews* 136, 117, <http://dx.doi.org/10.1007/s11214-007-9170-x>.
- MacNeice, P., Elliott, B., Acebal, A.O., 2011. Validation of community models: 3. Tracing fieldlines in heliospheric models. *Space Weather* 9, S10004, <http://dx.doi.org/10.1029/2011SW000665>.
- MacNeice, P., 2009. Validation of community models: 2. Development of a baseline using the Wang-Sheeley-Arge model. *Space Weather* 7, S06004, <http://dx.doi.org/10.1029/2009SW000463>.
- Neugebauer, M., Synder, C.W., 1966. Mariner 2 observations of the solar wind, 1. Average properties. *Journal of Geophysical Research* 71, 4469–4483.
- Nolte, J.T., Krieger, A.S., Roelof, E.C., Gold, R.E., 1977. High coronal structure of high velocity solar wind stream sources. *Solar Physics* 51, 459–471, <http://dx.doi.org/10.1007/BF00216379>.
- McComas, D.J., Bame, S.J., Barraclough, B.L., Feldman, W.C., Funsten, H.O., Gosling, J.T., Riley, P., Skoug, R., Balogh, A., Forsyth, R., Goldstein, B.E., Neugebauer, M., 1998. Ulysses' return to the slow solar wind. *Geophysical Research Letters* 25, 1–4, <http://dx.doi.org/10.1029/97GL03444>.
- McDonald, F.B., Ludwig, G.H., 1964. Measurement of low-energy primary cosmic ray protons on the IMP-1 satellite. *Physical Review Letters* 13, 783.
- McGregor, S.L., Hughes, W.H., Arge, C.N., Owens, M.J., Odstrčil, D., 2011. The distribution of solar wind speeds during solar minimum: calibration for numerical solar wind modeling constraints on the source of the slow solar wind. *Journal of Geophysical Research* 116, A03101, <http://dx.doi.org/10.1029/2010JA015881>.
- McKibben, R.B., Simpson, J.A., Zhang, M., Bame, S., Balogh, A., 1995. Ulysses out-of-ecliptic observations of "27-day" variations in high energy cosmic ray intensity. *Space Science Reviews* 72, 403–408, <http://dx.doi.org/10.1007/BF00768812>.
- Müller-Mellin, R., Kunow, H., Fleißner, V., Pehlke, E., Rode, E., Röschmann, N., Scharnberg, C., Sierks, H., Rusznayk, P., McKenna-Lawlor, S., Elendt, I., Sequeiros, J., Meziat, D., Sanchez, S., Medina, J., Del Peral, L., Witte, M., Marsden, R., Henrion, J., 1995. COSTEP – Comprehensive Superthermal and Energetic Particle analyser. *Solar Physics* 162, 483–504, <http://dx.doi.org/10.1007/BF00733437>.
- Murphy, N., Smith, E.J., Schwadron, N.A., 2002. Strongly underwound magnetic fields in co-rotating rarefaction regions: Observations and implications. *Geophysical Research Letters* 29, 23-1–23-4, <http://dx.doi.org/10.1029/2002GL015164>.
- Ness, N.F., Burlaga, L., 2001. Spacecraft studies of the interplanetary magnetic field. *Journal of Geophysical Research* 106 (A8), 15,803–15,817.
- Ness, N.F., Wilcox, J.M., 1964. Solar origin of the interplanetary magnetic field. *Physical Review Letters* 13, 461–464.
- Núñez, M., 2011. Predicting solar energetic proton events ($E > 10$ MeV). *Space Weather* 9, S07003, <http://dx.doi.org/10.1029/2010SW000640>.
- Odstrčil, D., Pizzo, V., 1999. Distortion of the interplanetary magnetic field by three-dimensional propagation of coronal mass ejections in a structured solar wind. *Journal of Geophysical Research* 104 (28,225).

- Odstřil, D., Riley, P., Zhao, X.P., 2004. Numerical simulation of the 12 May 1997 interplanetary CME event. *Journal of Geophysical Research* 109, A02116.
- Paizis, C., Heber, B., Ferrando, P., Raviart, A., Falconi, B., Marzolla, S., Potgieter, M.S., Bothmer, V., Kunow, H., Müller-Mellin, R., Posner, A., 1999. Amplitude evolution and rigidity dependence of the 26-day recurrent cosmic ray decreases: COSPIN/KET results. *Journal of Geophysical Research* 104, 28,241–28,248, <http://dx.doi.org/10.1029/1999JA900370>.
- Parker, E.N., 1958. Dynamics of the interplanetary gas and magnetic fields. *Astrophysics Journal* 128, 664–675.
- Pizzo, V.C., 1980. A three-dimensional model of co-rotating streams in the solar wind. 2: Hydrodynamic streams. *Journal of Geophysical Research*, 727–743.
- Pizzo, V.C., 1978. A three-dimensional model of corotating streams in the solar wind. 1: Theoretical foundations. *Journal of Geophysical Research* 83, 5563–5572.
- Posner, A., Hassler, D.M., McComas, D.J., Rafkin, S., Wimmer-Schweingruber, R.F., Böhm, E., Böttcher, S., Burmeister, S., Dröge, W., Heber, B., 2005. A high energy telescope for the Solar Orbiter. *Advances in Space Research* 36, 1426–1431, <http://dx.doi.org/10.1016/j.asr.2004.11.040>.
- Posner, A., Zurbuchen, T.H., Schwadron, N.A., Fisk, L.A., Gloeckler, G., Linker, J.A., Mikic, Z., Riley, P., 2001. Nature of the boundary between open and closed magnetic field line regions at the Sun revealed by composition data and numerical models. *Journal of Geophysical Research* 106 (A8), 15,869–15,880, <http://dx.doi.org/10.1029/2000JA000112>.
- Posner, A., 2007. Up to 1-h forecasting of radiation hazards from solar energetic ion events with relativistic electrons. *Space Weather* 5, S05001, <http://dx.doi.org/10.1029/2006SW000268>.
- Posner, A., 1999. Spuren quasi-stationärer heliosphärischer Struktur des solaren Minimums: SOHO/COSTEP- und Ulysses/COSPIN-Messungen CIR-assoziierter energiereicher Protonen. Ph.D. thesis, University of Kiel, Germany.
- Richardson, I.G., Wibberenz, G., Cane, H.V., 1996. The relationship between recurring cosmic ray depressions and corotating solar wind streams at ≤ 1 AU: IMP 8 and Helios 1 and 2 anticoincidence guard rate observations. *Journal of Geophysical Research* 101, 13,483–13,496, <http://dx.doi.org/10.1029/96JA00547>.
- Richardson, I.G., Barbier, L.M., Reames, D.V., von Roseninge, T.T., 1993. Corotating MeV/amu ion enhancements at 1AU or less from 1978 to 1986. *Journal of Geophysical Research* 98, 13–32, <http://dx.doi.org/10.1029/92JA01837>.
- Schwadron, N.A., 2002. An explanation for strongly underwound magnetic field in co-rotating rarefaction regions and its relationship to footpoint motion on the sun. *Geophysical Research Letters* 29, 8-1–8-4, <http://dx.doi.org/10.1029/2002GL015028>.
- Schwenn, R., 1990. Large-scale structure of the interplanetary medium. In: Schwenn, R., Marsch, E. (Eds.), *Physics of the Inner Heliosphere, 1: Large-scale Phenomena*. Springer-Verlag, Berlin, Germany, pp. 99–182.
- Smith, E.J., 2013. Large deviations of the magnetic field from the Parker spiral in CRRs: Validity of the Schwadron model. *Journal of Geophysical Research* 118, 58–62, <http://dx.doi.org/10.1002/jgra.50098>.
- Smith, E.J., Wolfe, J.H., 1979. Fields and plasmas in the outer solar system. *Space Science Reviews* 23, 217–252, <http://dx.doi.org/10.1007/BF00173811>.
- Sternal, O., Engelbrecht, N.E., Burger, R.A., Ferreira, S.E.S., Fichtner, H., Heber, B., Kopp, A., Potgieter, M.S., Scherer, K., 2011. Possible evidence for a Fisk-type heliospheric magnetic field. I. Analyzing Ulysses/KET electron observations. *Astrophysical Journal* 741, 23, <http://dx.doi.org/10.1088/0004-637X/741/1/23>.
- Veronig, A.M., Temmer, M., Vrsnak, B., Thalmann, J.K., 2006. Interaction of a Moreton/EIT wave and a coronal hole. *Astrophysical Journal* 647, 1466–1471, <http://dx.doi.org/10.1086/505456>.
- von Roseninge, T.T., Reames, D.V., Baker, R., Hawk, J., Nolan, J.T., Ryan, L., Shuman, S., Wortman, K.A., Mewaldt, R.A., Cummings, A.C., Cook, W.R., Labrador, A.W., Leske, R.A., Wiedenbeck, M.E., 2008. The High-Energy Telescope for STEREO. *Space Science Reviews* 136 (1–4), 319, <http://dx.doi.org/10.1007/s11214-007-9300-5>.
- Wang, Y.-M., Sheeley, N.R., 1993. Understanding the rotation of coronal holes. *Astrophysical Journal* 414, 916, <http://dx.doi.org/10.1086/173135>.
- Wawrzynczak, A., Modzelewska, R., Alania, M.V., 2011. Three-dimensional model of the interplanetary magnetic field and 27-day variation of the galactic cosmic ray intensity. *Astrophysics and Space Sciences Transactions* 7, 351–354, <http://dx.doi.org/10.5194/asttra-7-351-2011>.
- Zeitlin, C., Boynton, W., Mitrofanov, I., Hassler, D.M., Atwell, W., Cleghorn, T.F., Cucinotta, F.A., Al-Dayeh, M., Desai, M.I., Guetersloh, S.B., Kozarev, K., Lee, K.T., Pinsky, L., Saganti, P., Schwadron, N.A., Turner, R., 2010. Mars Odyssey measurements of galactic cosmic rays and solar particles in Mars orbit, 2002–2008. *Space Weather* 8, S00E06, <http://dx.doi.org/10.1029/2009SW000563>.
- Zhang, A., 1997. Linear relationship between the latitude gradient and 26 day recurrent variation in the fluxes of galactic cosmic rays and anomalous nuclear components. I. Observations. *Astrophysical Journal* 488, 841, <http://dx.doi.org/10.1086/304732>.
- Zirker, J.B., 1977. Coronal holes and high-speed wind streams. *Reviews of Geophysics and Space Physics* 15, 257–269, <http://dx.doi.org/10.1029/RG015i003p00257>.